RESERCH ARTICLE

EARTH SCIENCES

Anthropogenic emissions are the main contribution to the rise of atmospheric methane (1993-2017)

Zhen Zhang (张臻)[1*], Benjamin Poulter[2], Sara Knox[3], Ann Stavert[4], Gavin McNicol[5], Etienne Fluet-Chouinard[6], Aryeh Feinberg[7], Yuanhong Zhao (赵园红)[8], Philippe Bousquet[9], Josep G. Canadell[4], Anita Ganesan[10], Gustaf Hugelius[11], George Hurtt[1], Robert B. Jackson[6,12], Prabir K. Patra[13], Marielle Saunois[9], Lena Höglund-Isaksson[14], Chunlin Huang (黄春林)[15], Abhishek Chatterjee[16,17], Xin Li (李新)[18]

[1]Department of Geographical Sciences, University of Maryland, College Park, MD 20742, USA

[2]Biospheric Sciences Laboratory, NASA Goddard Space Flight Center, Greenbelt, MD 20771, USA

[3]Department of Geography, University of British Columbia, Vancouver, V6T 1Z2, Canada

[4]Global Carbon Project, CSIRO Oceans and Atmosphere, Canberra, ACT 2601, Australia

[5]Department of Earth and Environmental sciences, University of Illinois Chicago, Chicago, IL 60607, USA

[6]Department of Earth System Science, Stanford University, Stanford, CA 94305, USA

[7]Institute for Data, Systems, and Society, Massachusetts Institute of Technology, Cambridge, MA 02139, USA

[8]College of Oceanic and Atmospheric Sciences, Ocean University of China, Qingdao, 266000, China

[9]Laboratoire des Sciences du Climat et de l'Environment, LSCE-IPSL (CEA-CNRS-UVSQ), Université Paris-Saclay 91191 Gif-sur-Yvette, France

[10]School of Geographical Sciences, University of Bristol, Bristol, BS8 1RL, UK

[11]Department of Physical Geography and Bolin Centre for Climate Research, Stockholm University, Stockholm, SE-106 91, Sweden

[12]Woods Institute for the Environment and Precourt Institute for Energy, Stanford University, Stanford, CA 94305, USA

[13]Research Institute for Global Change, JAMSTEC, 3173-25 Showa-machi, Kanazawa-ku, Yokohama 236-0001, Japan

[14]International Institute for Applied Systems Analysis (IIASA), Laxenburg, A-2361, Austria

[15]Northwest Institute of Eco-Environment and Resources, Chinese Academy of Sciences, Lanzhou, 730000, China

[16]Global Modeling and Assimilation Office, NASA Goddard Space Flight Center, Greenbelt, MD 20771, USA

[17]Universities Space Research Association, Columbia, MD 21046, USA

[18]Institute of Tibetan Plateau Research, Chinese Academy of Sciences, Beijing, 100101, China

*Corresponding author: Zhen Zhang. **Email:** yuisheng@gmail.com

Abstract: Atmospheric methane (CH_4) concentrations have shown a puzzling resumption of growth since 2007 following a period of stabilization from 2000 to 2006. Multiple hypotheses have been proposed to explain the temporal variations in CH_4 growth, which attributes the rise of atmospheric CH_4 either to increases in emissions from fossil fuel activities, agriculture, and natural wetlands or to a decrease in the atmospheric chemical sink. Here, we use a comprehensive ensemble of CH_4 source estimates and isotopic $\delta^{13}C$-CH_4 source signature data to show that the resumption of CH_4 growth is most likely due to increased anthropogenic emissions. Our emission scenarios that have the fewest biases with respect to isotopic composition suggest that the agriculture, landfill, and waste sectors were responsible for 53±13% of the renewed growth over the period 2007-2017 compared to 2000-2006; industrial fossil fuel sources explained an additional 34±24%, and wetland sources contributed the least at 13±9%. The hypothesis that a large increase in emissions from natural wetlands drove the decrease in atmospheric $\delta^{13}C$-CH_4 values cannot be reconciled with current process-based wetland CH_4 models. This finding suggests the need for increased wetland measurements to better constrain the contemporary and future role of wetlands in the rise of atmospheric methane and climate feedbacks. Our findings highlight the predominant role of anthropogenic activities in driving the growth of atmospheric CH_4 concentrations.

Keywords: greenhouse gas, carbon cycle, climate mitigation, wetland, methane isotope

Introduction

Stabilizing atmospheric methane (CH_4) emissions from anthropogenic activities is a critical component of climate change mitigation [1]. The atmospheric CH_4 concentration has increased approximately 2.5-fold from 731 ppb (parts per billion) in 1750 (preindustrial reference year [2]) to 1890 ppb in 2020 [3]. Meanwhile, over the past century, atmospheric $\delta^{13}C$-CH_4 values increased from ~ -49.0‰ in 1912 to -47.2‰ in 2007 due to increasing emissions of isotopically ^{13}C-enriched (i.e., isotopically heavy) fossil fuels [4]. Despite the importance of understanding the temporal changes in atmospheric CH_4, the drivers of changes in the growth rate of atmospheric CH_4 over recent decades remain poorly understood [5]. The increase in atmospheric CH_4 slowed in the early 1990s followed by a so-called stabilization period during 2000-2006[6]. Since 2007, global atmospheric CH_4 concentrations began to rise again, accompanied by a decline in $\delta^{13}C$-CH_4 values from -47.2‰ in 2007 to -47.4‰ in 2017 [3]. The cause of this change has been studied recently using atmospheric inversion models [7–10], atmospheric box models [11–15], and emission inventories [16]. These studies have arrived at divergent and even conflicting conclusions [17], evoking increasing emissions of CH_4 from fossil fuels, agriculture, wetlands, and/or decreased hydroxyl radicals (OH) as main drivers due to different measurements, methodologies and time periods considered (see Materials and Methods). Such discrepancies highlight the need to reconcile our understanding of the drivers of the growth in atmospheric CH_4 for the design of mitigation policies [18].

Sources in the global CH_4 budget are mainly determined by three broadly defined groups: 1) thermogenic sources from industrial fossil fuel (e.g. coal, oil and natural gas; IFF_{CH4}) and geological sources (GEO_{CH4}); 2) biogenic sources from livestock, rice agriculture, landfills and waste (AGW_{CH4}) and natural wetlands (WET_{CH4}); and 3) pyrogenic sources from wildfires and biomass burning (BB_{CH4}). The primary sink for CH_4 is reactions with tropospheric hydroxyl radicals (OH), soil microbial uptake, and a small contribution from tropospheric chlorine reactions, which affect the isotopic compositions. The shift of the trend in atmospheric $\delta^{13}C$-CH_4 values towards more ^{13}C-depleted (i.e., isotopically light) compositions suggests a higher dominance of isotopically light biogenic emissions in the global CH_4 budget [11, 19]. This hypothesis has been supported by a few recent process-based and inversion modeling which point to either a systematic underestimation of AGW_{CH4} [20] or a large increase in WET_{CH4} [8,10,21,22]. In contrast, there are large differences in the rate of change across inventory-based estimates of industrial fossil fuel source activity IFF_{CH4} [23,24], as well as substantial underestimates in some regions and overestimates in other regions [12,25,26]. Globally, studies suggests that BB_{CH4} has been declining, with fire CH_4 emissions associated with an isotopically enriched signature, thus providing room in the isotopic budget for an increase in fossil fuel sources [13]. GEO_{CH4}, which is often co-located with the fossil fuel industry, is suggested to be largely overestimated by recent studies [27,28], indicating a potentially larger role of IFF_{CH4} in affecting the global CH_4 budget given its underestimated share of the total CH_4 source [12,29].

OH oxidation in the troposphere is the main CH_4 sink, and reactions with chlorine (Cl), stratospheric sinks, and soil removal are small-magnitude sinks. Substantial difficulties remain in quantifying CH_4 sinks, especially the main chemical sink for CH_4, tropospheric OH [5]. OH plays a significant but ambiguous role in driving the

observed atmospheric trend; it is difficult to estimate due to its complicated chemistry, i.e., nonlinear chemical feedbacks, and short lifetime [30,31]. For example, estimates of interannual variability (IAV) in global mean OH are significantly higher in the empirical box model estimates that use CO and methylchloroform (MCF) constraints [32] than estimates based on chemical transport models (Fig. S1). Although there are debates on the potential biases in the box-model-based OH due to ignorance of complex spatial heterogeneity in OH and transport [33,34], the uncertainties in OH trends and variability are likely large enough to explain any potential CH_4 growth scenarios [14,15,35]. In addition, the trends in OH exert isotopic leverage on atmospheric $\delta^{13}C\text{-}CH_4$ values via the kinetic fractionation effect, such that increasing OH increases the atmospheric $\delta^{13}C\text{-}CH_4$ value by reacting with more $^{12}CH_4$. Therefore, it is of interest to investigate hypotheses regarding CH_4 sources with atmospheric $\delta^{13}C\text{-}CH_4$ observations while assuming that these sources can reproduce the atmospheric records with varying OH.

A thorough investigation of these hypotheses in a clearly defined framework is essential to help resolve the unexplained change in the growth rate of atmospheric CH_4. Here, we use an isotopic mass balance approach to attribute drivers of the growth rate of atmospheric CH_4 using i) a large ensemble of scenarios to represent different combinations of emissions hypotheses (denoted emission scenarios, see Materials and Methods) from a comprehensive set of updated bottom-up estimates representing anthropogenic emission inventories and spatially explicit signatures for major CH_4 sources. Each emission scenario is composed of a time series of sectoral CH_4 fluxes and their hemispheric emission-weighted $\delta^{13}C\text{-}CH_4$ values. A globally representative database and spatially resolved distributions of $\delta^{13}C\text{-}CH_4$ values for the major CH_4 sources [36–38] were used to evaluate the temporal and regional variability in observed $\delta^{13}C\text{-}CH_4$ values. Monte Carlo techniques were applied to explore the uncertainty in $\delta^{13}C\text{-}CH_4$ estimates with full consideration of the spatial heterogeneity in CH_4 sources and their $\delta^{13}C\text{-}CH_4$ signatures. Scenario-specific parameters for the time series of the CH_4 removal rate driven by OH variations and run-specific $^{13}CH_4$ fractionation factors were derived by inverting an atmospheric two-box model (see Methods and Supplementary Materials). We then evaluate the emission scenarios against observed $\delta^{13}C\text{-}CH_4$ values for 1993-2017 by running the two-box model in the forward mode. To test the hypothesis of large increase from wetland CH_4 emission, the idealized wetland scenarios (i.e. without process-based constraint) are then calculated to reproduce the temporal pattern of $\delta^{13}C\text{-}CH_4$. The comparison against atmospheric isotopic observations allowed us to select the most likely set of emission scenarios, which are defined as the 1st percentile cutoff of the lowest mean squared difference (MSD) in simulated $\delta^{13}C\text{-}CH_4$ values.

Results and discussion

Temporal variations in the atmospheric CH_4 concentration and its $\delta^{13}C\text{-}CH_4$ value

The ensemble simulations for the 96 emission scenarios (4 IFF_{CH4} x 3 AGW_{CH4} x 2 WET_{CH4} x 2 BB_{CH4} x 2 GEO_{CH4}) reproduced the observed atmospheric CH_4 concentration (Fig. 1A) using the corresponding optimized time series of OH derived from running the box model in inverse mode (Fig. S1). We accounted for the uncertainty in source signatures of $\delta^{13}C\text{-}CH_4$ by resampling 1000 sets of $\delta^{13}C\text{-}CH_4$ signature time series for each emission scenario (N = 96 x 1000), which resulted in a wide range of modeled atmospheric $\delta^{13}C\text{-}CH_4$ values with some closely reproducing the observations. However, most of emission scenarios tended to generate more enriched $\delta^{13}C\text{-}CH_4$ trends for 1993-2017, suggesting that existing bottom-up inventories overestimate the increase in IFF_{CH4} during the study period, especially during slowdown and stagnation periods (Fig. 1B). Furthermore, to balance the rise in CH_4 sources, the increases in OH levels also led to positive trends in atmospheric $\delta^{13}C\text{-}CH_4$ values during these two periods (Fig. S1). Note that the large increase in coal-related emissions since 2003 has increased the $\delta^{13}C\text{-}CH_4$ values of the sources, which contribute to the divergence between the model and observations. The timing of this divergence is consistent with a rapid increase in methane emissions from China (mainly coal emissions) as reported by the inventories [23] and inversions [39]. For most of the emission scenarios, the estimated temporal variations in OH for 1993-2017 fall within the 1-σ range of the Bayesian inversion from [14] and are in good agreement with [35] for the post-2000 period. The EDGARv4.2-based emission scenarios have the largest mismatch with the inversion-based OH anomaly (relative to a global mean concentration of 1e^6 molecules (molec)/cm^3), confirming the known higher bias in EDGARv4.2 than in other inventories (Fig. S2).

The time series of CH_4 sources for 1993-2017 (Fig. 1C) suggests that decadal-scale variations in atmospheric CH_4 are dominated by anthropogenic emissions from both agricultural and fossil fuel activities. However, there is high uncertainty across IFF_{CH4} inventories, with a sizable (> 40 Tg CH_4 yr^{-1}) difference in magnitude and a

large difference in temporal trends between inventories (i.e., EDGARv4.2, EDGARv4.3.2, and GAINS) and an atmospheric-observation-constrained approach (i.e., SCH150, which hypothesizes that IFF_{CH4} is underestimated but does not increase over time). The temporal variation in AGW_{CH4} exhibits a lower discrepancy than IFF_{CH4} in the inventories, whereas WET_{CH4} and BB_{CH4} are more constrained. The IAV and magnitude of our estimates for WET_{CH4} calculated using the process-based model LPJ-wsl is comparable to the ensemble mean of multiple wetland models [40] and a global wetland CH_4 emission model ensemble for use in atmospheric chemical transport models (WetCHARTs) [41]. The wetland CH_4 estimates derived from driving the wetland model with a ground-measurement based meteorological dataset from the Climate Research Unit (denoted CRU) yield a small increase (< 1 Tg CH_4 yr^{-1}), whereas the same model with climate reanalysis (denoted REN) has an ~7.3 Tg CH_4 step increase from tropical wetlands between 2000-2006 and 2007-2017 [22].

Evaluations of the proposed CH_4 hypotheses by using emission scenarios

Fig. 2A shows the distribution of residual bias in the individual box model simulations in terms of how they reproduce the observed $\delta^{13}C$-CH_4 values. In the Taylor diagram [42] the global average $\delta^{13}C$-CH_4 values of the sources before fractionation by chemical sinks range from -53‰ to -55‰ over 1993-2017, and a correlation coefficient lower than 0.6 is obtained for all of the simulations for 1993-2017. The low agreement suggests that the biases in the inventories and the wetland models contribute to the discrepancies in reproducing the $\delta^{13}C$-CH_4, which is likely due to the overestimated increase in inventories, especially the coal emission that has relatively heavy isotopic signature, as found by previous atmospheric inversion studies [16]. In addition, some of the simulations can reproduce similar IAV in atmospheric $\delta^{13}C$-CH_4 values with root mean square errors (RMSEs) from 0.05‰ to 0.5‰, but ~85% of simulations tend to produce higher IAV than observed. Although the global average $\delta^{13}C$-CH_4 value was regarded as observational 'truth', this reference has an uncertainty of 0.04‰, attributed to variability in measurements across all the stations and uncertainty from scale conversions between networks [43].

The density distributions of RMSEs grouped by different bottom-up CH_4 estimates show the divergent performance of emission scenarios in reproducing observed atmospheric $\delta^{13}C$-CH_4 values (Fig. 2B). Among the four IFF_{CH4} inventories, 80% of simulations using EDGARv4.2 generated more positive trends of $\delta^{13}C$-CH_4 values than the other three inventories, with no EDGARv4.2-based runs located in the most likely set of emission scenarios (Fig. S3). This result corroborates previous studies that also suggest that EDGARv4.2 tends to overestimate fossil fuel growth [44]. The more recent EDGARv4.3.2 has been improved, with 95% of the simulations located within the RMSE range from 0.1‰ to 0.3‰, mainly due to improved emission factors and revised statistics of CH_4 sectors [23]. SCH150 produces lower agreement than EDGARv4.3.2 due partly to the low IAV of SCH150, as SCH150 focuses on the long-term trends in IFF_{CH4}. The GAINS inventories generated better performance: 78% of the simulations in the 1st percentile of MSD are based on GAINS IFF_{CH4}. Note that this does not rule out the IFF_{CH4} scenarios that have flat or insignificant trends (e.g., SCH150), as ^{13}C-enriched BB_{CH4} estimates in this study show declining trends over recent years, which would allow for compensation by increasing emissions from IFF_{CH4} to meet the decreasing atmospheric $\delta^{13}C$-CH_4 values. Generally, IFF_{CH4} has a more pronounced impact in determining the past trends in $\delta^{13}C$-CH_4 changes than the other major CH_4 sources.

The contribution of combined agriculture, landfills and waste included in AGW_{CH4}, which together represent 50%-62% of the total anthropogenic sources, again reveals a higher bias of EDGARv4.2-based simulations compared to the other two inventories (Fig. 2B). Agricultural emissions dominate AGW_{CH4}, with an average contribution of 77.5% to the total AGW_{CH4} over the study period. The lower MSD scores using EDGARv4.3.2 and WOLF2017 emission scenarios show improved reconciliation of estimates for the AGW_{CH4} source relative to the isotopic budget. This result supports the hypothesis that the global livestock estimates based on the 2006 IPCC Tier 1 guidelines underestimate livestock CH_4 emissions at the national or state level [45], which is potentially attributable to outdated information used to develop the emission factors. However, there is no clear signal to distinguish whether EDGARv4.3.2 or WOLF2017 has a lower a priori bias, suggesting the need for further regional and global assessments by spatially explicit 4-D atmospheric models.

Our calculations suggest that, in contrast to anthropogenic sources, wetland CH_4 emissions play a limited role in reproducing the decadal trend in atmospheric $\delta^{13}C$-CH_4 (Fig. 1; Fig. 2B). Both REN and CRU demonstrate that wetland CH_4 emissions appear to have contributed little to the renewed growth in atmospheric CH_4. However, wetland emissions help explain the IAV in the atmospheric CH_4 growth rate via its pulsed responses to climate dynamics, such as the El Niño-Southern Oscillation [46]. The latitudinal gradient of the growth rate for CH_4 sources (Fig. S4) suggests that WET_{CH4} in the tropics has an important impact on the IAV of the CH_4 growth

rate, albeit the current limited understanding of WET_{CH4} is due to a significant deficiency in WET_{CH4} measurements in the tropics, especially for Africa [21].

The density distribution of RMSE grouped by BB_{CH4} and GEO_{CH4} (Fig. 2B) suggests that the recent hypotheses regarding a larger decrease [13] in BB_{CH4} and overestimated contemporary GEO_{CH4} [27,28] have a good agreement with the isotopic budget. The lower RMSE of Worden (2017)-based scenarios supports the hypothesis of a decreasing trend in BB_{CH4} during the post-2007 period, as suggested by inversion modeling based on satellite measurements of carbon monoxide [47]. The low GEO_{CH4} scenarios, which assume a geological source of 15 Tg CH_4 yr^{-1} with upward-revised IFF_{CH4} (see Methods and Supplementary), yield lower RMSEs than the conventional high-GEO_{CH4} scenarios in which GEO_{CH4} was set to 52 Tg CH_4 yr^{-1}. These findings support the hypothesis that the current bottom-up estimates of anthropogenic fossil fuel CH_4 emissions are underestimated and that geological emissions are overestimated.

Changes in the trends of δ^{13}C-CH_4 source signatures

A change in source signature (Fig. 3A) suggests varying global emission-weighted average source signatures driven by the change in spatiotemporal distribution of CH_4 source estimates for the four major CH_4 categories. When considering spatial heterogeneity in the source signature, the globally representative δ^{13}C-CH_4 values tend to suggest a larger variation than previous assumptions that use globally uniform values [7,13]. The IFF_{CH4} signature varies between time periods from a median of -44.9‰ during 2000-2006 to a median of -42.7‰ during 2013-2017, suggesting high variability in the δ^{13}C-CH_4 values of anthropogenic CH_4 sources. The AGW_{CH4} signature slightly increased from a median value of -62.5‰ to -62.3‰ from 2000-2006 to post-2007. Note that the effect of the decreasing trend of atmospheric δ^{13}C-CO_2 values on the C_3-C_4 diet composition of domestic ruminants in recent decades was not taken into account in this study; consideration of this factor would yield a slight decrease in the AGW_{CH4} signature [48]. Wetland δ^{13}C-CH_4 values increased slightly from -59.7‰ to -59.5‰ from the stabilization period to the renewed-growth period, mainly attributable to increased tropical wetland CH_4 emissions since 2007. Tropical wetlands tend to have a more enriched signature (mean -56.7‰) than northern high-latitude peatland-based wetlands (mean -67.8‰) (Fig. S5), as supported by a few site-level measurements [36,38,49]. The possible signature enrichment from wetlands is another line of evidence for a weak wetland CH_4 emission response [22,40], while there is no evidence of a significant change in wetland CH_4 from high latitudes in either model [16,44] or by direct atmospheric measurement [50], where the rise of WET_{CH4} may possibly be counteracted by increased soil uptake [51]. However, it is difficult to distinguish CH_4 from wetlands and livestock, as the signatures of the two sectors are similar and the spatial distributions are possibly co-located [3], suggesting a critical need for more measurements to provide better constraints on δ^{13}C-CH_4 values in the tropics.

The change in the δ^{13}C-CH_4 contribution from individual sources does not necessarily imply the same trend in the global average signature. Theoretically, even if the tropical wetland signature becomes more positive, the increased proportion of wetland-contributed $^{13}CH_4$ mass to the total $^{13}CH_4$ mass can still result in a shift towards a more negative global signal, as the biogenic signature is considerably lighter than the global atmospheric δ^{13}C-CH_4 value [36] (~ -53.6‰) before fractionation. This is the case in some paleoclimate studies [52] where tropical wetlands and other natural sources (e.g., biomass burning) dominated the annual CH_4 budget. However, the role of human activities has become dominant in the annual CH_4 and isotope budgets since 1750 A.D., and the relative importance of wetlands has lessened. Fig. 3B also shows the probability distribution of the relative contribution of $^{13}CH_4$ mass to the annual total $^{13}CH_4$ mass in the source from 2000-2006 to the post-2007 period. IFF_{CH4} exhibits either an increased contribution of 5-8% based on EDGARv4.2 or a decreased contribution of 6-9% relative to 2000-2006 based on SCH150 or GAINS. In contrast to IFF_{CH4}, AGW_{CH4} shows a significantly increasing contribution to the isotope budget from 2000-2006 to the post-2007 period, with a positive trend of 5-7% relative to 1993-1999. This pattern can be explained by the substantial increase in AGW_{CH4} production since the 21st century. The contribution from BB_{CH4} to the $^{13}CH_4$ mass was 20-25% lower in 2007-2017 than in 1993-1999 and 2000-2006, mainly due to reduced biomass burning, as suggested by the inversion model based on satellite retrievals [13] and by inventories [47].

Idealized wetland emission scenarios that reproduce the decrease in atmospheric δ^{13}C-CH_4 values

Beyond our wetland-model ensemble, we created scenarios to investigate the possibility of rising WET_{CH4} in reproducing the decrease in atmospheric δ^{13}C-CH_4 values. To do so, we performed a sensitivity test by running the box model in inverse mode for each individual run to calculate idealized WET_{CH4} given the other sources, varying OH concentration, atmospheric CH_4 and δ^{13}C-CH_4 observations, and the isotopic signatures of the sources, which thus linearizes the problem. The results suggest that the magnitude of increase in idealized

WET_{CH4} largely depends on the hypothesis of IFF sources, where greater wetland increases are required to compensate for the large increase in the IFF_{CH4} scenarios (Fig. 4A). Note that all the idealized WET_{CH4} scenarios are higher than the two WET_{CH4} scenarios in this study (i.e., CRU and REN) or WetCHARTs, which is based on satellite-derived surface water extent and precipitation reanalysis and an ensemble of ecosystem respiration estimates. One process-based WET_{CH4} that overlaps the increases in idealized wetland scenarios is the ensemble mean of LPJ-wsl simulations for a future projection under the climate scenario RCP8.5 [53] (denoted Zhang2017). RCP8.5 is considered the upper bound of wetland CH_4 feedback to rising temperature in LPJ-wsl because the strong and steady increase in temperature in RCP8.5 is higher than that determined from actual observations. Note that this scenario would occur only in combination with the hypothesis that IFF_{CH4} has had no significant trends in recent years.

The comparison of 2000-2017 trends in WET_{CH4} (Fig. 4B) suggests that to reproduce the magnitude of the observed decrease in atmospheric $\delta^{13}C\text{-}CH_4$ values, the required emission increase from natural wetlands would need to be much higher than the current estimates from process-based wetland models. The trend of CRU is consistent with the ensemble estimate of global wetland model simulations [5,40], while that of REN is at the higher end of the trends that consider the potential inundation increase due to enhanced tropical precipitation [22]. Note that the range of idealized increases in WET_{CH4} is in line with two recent inversion studies [8,10] based on GOSAT CH_4 measurements, which suggests a positive wetland trend of 2-3 Tg CH_4 yr^{-1} yr^{-1} for 2010-2018. However, to produce such a significant trend, the Q10 parameter (temperature sensitivity of CH_4 emissions) in the wetland models would need to be much higher than the range of 2-3 from LPJ-wsl and WetCHARTs or the measurement-based average of 2.57 from FLUXNET-CH4 [54]. In addition, a recent multi-model ensemble inversion study [55] suggests that the observation-constrained wetland CH_4 feedback to rising temperature is lower than that of Zhang2017. Despite this, there are considerable uncertainties in modelled WET_{CH4} due to scarcity of measurements for the tropics [40]. We conclude that the hypothesis of a large increase from natural wetlands driving the decrease in atmospheric $\delta^{13}C\text{-}CH_4$ values cannot be reconciled with process-based wetland CH_4 models.

Attributions of CH_4 rise based on the most likely scenarios

Our Monte Carlo estimation (Table 1) suggests that the largest uncertainties in global representative source $\delta^{13}C\text{-}CH_4$ values are from industrial fossil fuel activities, providing clues for future studies. Our estimated global representative values for total CH_4 source signatures are within the uncertainty of recently compiled databases [12,36] but are lower than the value used in previous inverse studies (see Fig. S6 for references). Among the major CH_4 emission sectors, the global average emission-weighted $\delta^{13}C\text{-}CH_4$ signature for coal has the highest IAV, which is mainly due to the large deviation in country-level data in coal emissions [39] and the heterogeneous distribution of different coal ranks [56]. Note that the low-rank coals tend to produce isotopically lighter CH_4 [36] with a potentially biogenic origin [57], indicating that the proportion of consumption of different coal types may have a significant impact on atmospheric $\delta^{13}C\text{-}CH_4$ values.

We calculate the most likely scenarios based on the agreement of bottom-up estimates with isotopic observations (Fig. 5). The results suggest that the agricultural, landfill and waste sectors account for 53±13% (21.0±0.8 Tg CH_4 yr^{-1}; 1-σ) of renewed growth over the period of 2007-2017 compared to 2000-2006, with industrial fossil fuel sources and wetland sources contributing 34±24% (13.7±8.8 Tg CH_4 yr^{-1}) and 13±9% (5.3±3.5 Tg CH_4 yr^{-1}), respectively. The decreasing emissions from fossil fuel sectors in 1993-1999 compared to 2000-2006, combined with the increasing OH anomaly (Fig. S8), may have contributed to the CH_4 stabilization period (Fig. 5 and Fig. S7). The increases in methane emissions (mainly from the fossil fuel, agriculture, and waste sectors) combined with a step increase from wetland CH_4 and small decreases in OH levels lead to renewed growth in methane during 2007-2012. Moreover, the higher CH_4 emissions from mainly anthropogenic activities, i.e., coal, oil and gas, livestock, and landfill and waste sectors, drove the accelerated increase in atmospheric CH_4 during 2013-2017. These sectoral emission increases are consistent with economic activity data (Table S2; Table S3) showing that, in the past decade, coal production has increased by 41.7% globally (International Energy Agency, https://www.iea.org/topics/coal/statistics/, last access Feb. 22, 2021) and that the populations of major livestock species (e.g., swine, chickens, and ruminant animals) have increased by 22.5% (FAOSTAT, http://www.fao.org/faostat/, last access Feb 22, 2021). Although coal production exhibited a temporary decline during 2014-2016 (https://www.bp.com/content/dam/bp/business-sites/en/global/corporate/pdfs/energy-economics/statistical-review/bp-stats-review-2020-full-report.pdf, last access Feb. 22, 2020), the average coal emissions during 2013-2017 were higher than those during 2007-2012, indicating that coal mining emissions continued to grow, with a higher contribution to the increase in atmospheric CH_4.

Conclusions

Our analysis shows that a comprehensive evaluation of hypotheses regarding the attribution of rising atmospheric CH_4 based on a combination of bottom-up approaches and isotopic values can reconcile multiple lines of evidence into a robust global CH_4 budget. However, we acknowledge that there are some biases and uncertainties in the bottom-up estimates and that our exploration of possible emission scenarios does not cover all potential scenarios. This study clearly suggests that the proposed hypotheses are influenced by the choice of a priori estimates, indicating that the high-bias a priori estimates of trends applied in some earlier studies have led to equally biased conclusions regarding the attribution of atmospheric methane rise. Our results suggest that decreasing emissions from coal, oil and gas from 1993-1999 to 2000-2006, combined with the increasing OH anomaly, likely contributed to the methane stabilization period. Anthropogenic sources were the most likely major contributor to the renewed growth in CH_4 after 2006. Moreover, the good agreement of low present-day geological source estimates with observations supports the hypothesis that the IFF_{CH4} in recent decades has been largely underestimated. However, our understanding of the role of livestock and wetlands, and particularly in tropical regions, is more limited, especially [58, 59]. Aircraft measurements in these regions may help address the lack of data and improve our understanding of WET_{CH4}. This study highlights the dominant role of anthropogenic emissions from fossil fuels, agriculture, landfills and waste in driving the recent rising trend in atmospheric CH_4. This study improves the understanding of causes of the changes in atmospheric CH_4 over the past 25 years, enabling the development of more targeted mitigation strategies and policies to stabilize and ultimately reduce key contributing emission sectors.

Materials and Methods

Model descriptions. The model was developed from previous studies [15,60,61] and consists of two perfectly mixed boxes representing the troposphere in the Northern and Southern Hemispheres. The changes in CH_4 concentration are calculated using the following equations:

$$^{12}CH_4^N(t+\Delta t) = {}^{12}CH_4^N(t) + \left(\sum_i {}^{12}S_i^N(t) + \sum_j k_j^{12}\,{}^{12}CH_4^N(t) - \frac{1}{2\tau_{ex}}\,{}^{12}CH_4^N(t) + \frac{1}{2\tau_{ex}}\,{}^{12}CH_4^S(t)\right)\Delta t \quad (1)$$

$$^{12}CH_4^S(t+\Delta t) = {}^{12}CH_4^S(t) + \left(\sum_i {}^{12}S_i^S(t) + \sum_j k_j^{13}\,{}^{12}CH_4^S(t) - \frac{1}{2\tau_{ex}}\,{}^{12}CH_4^S(t) + \frac{1}{2\tau_{ex}}\,{}^{12}CH_4^N(t)\right)\Delta t \quad (2)$$

where $^{12}CH_4$ is approximated by CH_4 and $^{12}S_i^N$(t) and $^{12}S_i^S$ (t) represent the annual source strength of the source in the Northern Hemisphere and Southern Hemisphere, respectively. k^{12} is the first-order removal rate coefficient for the sinks. The interhemispheric exchange time τ is set to a constant value of 1 yr given that the overall methane CH_4 concentration and OH anomalies are largely unaffected by the interhemispheric exchanges [15].

The δ^{13}C-CH_4 isotopic signatures of the different source categories i and the kinetic isotope effect (KIE) in the individual sink reactions j are used to calculate the sources ($^{13}S_i$) and removal rate coefficients ($^{13}k_j$) for δ^{13}C-CH_4 values:
where $13R_{std}$ = 1.12372% is the $^{13}C/^{12}C$ ratio of the international reference material Vienna Pee Dee Belemnite (VPDB). These terms are then used to derive the mixing ratio changes in ^{13}C-CH_4:

$$^{13}CH_4^N(t+\Delta t) = {}^{13}CH_4^N(t) + \left(\sum_i {}^{13}S_i^N(t) + \sum_j k_j^{13}\,{}^{13}CH_4^N(t) - \frac{1}{2\tau_{ex}}\,{}^{13}CH_4^N(t) + \frac{1}{2\tau_{ex}}\,{}^{13}CH_4^S(t)\right)\Delta t \quad (3)$$

$$^{13}CH_4^S(t+\Delta t) = {}^{13}CH_4^S(t) + \left(\sum_i {}^{13}S_i^S(t) + \sum_j k_j^{13}\,{}^{13}CH_4^S(t) - \frac{1}{2\tau_{ex}}\,{}^{13}CH_4^S(t) + \frac{1}{2\tau_{ex}}\,{}^{13}CH_4^N(t)\right)\Delta t \quad (4)$$

The mixing ratios of the individual isotopologues are converted to δ values as follows:

$$\delta_C^{13} = \left(\frac{^{13}CH_4/^{12}CH_4}{^{13}R_{std}} - 1\right) \quad (5)$$

The soil sink is considered to have a low IAV, as suggested by biogeochemical models [62,63], despite a recent study [64] based on a few site-level measurements suggesting a decline in the soil sink in temperate forests in recent decades. For soil CH_4 uptake, we use climatology from a process-based model [63] in the calculation of the hemispheric net CH_4 source (see equation 6 in Materials and Methods). The contributions of Cl sink and

stratospheric loss to the removal of CH_4 in the troposphere are highly uncertain and not well constrained by direct observations but has a strong kinetic isotope effect on $^{13}CH_4$. Given the large uncertainty in Cl and stratospheric sinks and the lack of available datasets, the magnitudes of these two sinks were not explicitly considered in the calculation of the hemispheric CH_4 budget. We assume that the annual methane removal rate is driven solely by OH variability, while other minor sinks are kept constant over the study period. Because sensitivity tests [65] suggest that the uncertain magnitude of Cl fields leads to a wide range of simulated $\delta^{13}C$-CH_4 values given its strong "isotope leverage" effect [66] (-60±1‰) on total ε, the sink-weighted average fractionation factor ε is highly uncertain. The approach in this study is to estimate the total ε value for each box model run that optimizes the match between atmospheric observations and simulation at the onset of the study period. The optimized ε values were derived from running the box model in inverse mode by matching the observed global average [11]. This allows us to explore the uncertainty in ε based on bottom-up source aggregation and the uncertainty in $\delta^{13}C$-CH_4 values. Fig. S6 shows that the estimated fractionation factors for the full ensemble and 1st percentile ensemble are broadly in agreement with previous studies [11–13,60,66–70]. The distribution of the mean methane lifetime (Fig. S9) over the study period is slightly lower than the estimated 9.1±0.9 yr from [71] and is comparable in magnitude to that between atmospheric chemistry-transport models in the recent model intercomparison [31,32,72]. Here, we evaluate the global results from the box model, instead of hemispheric results, to minimize the potential influence of uncertainty in IAV from interhemispheric transport on box model performance, as suggested by a recent study [73]. See SI for details about the model strategy.

CH_4 source estimates. To test all the proposed competing hypotheses, we carried out simulation experiments using box modeling for different emission scenarios based on a suite of bottom-up datasets. We first list all the possible options for the CH_4 inventories by five CH_4 source categories (i.e., IFF_{CH4}, AGW_{CH4}, WET_{CH4}, BB_{CH4}, and GEO_{CH4}) and then generate emission scenarios with combinations of CH_4 inventories. The assignment of the inventory (i.e., EDGAR)-specific sectors into the main categories IFF_{CH4}, AGW_{CH4} and BB_{CH4} follow the criteria from Supplement Table S4 in [5]. Anthropogenic CH_4 emissions related to fossil fuels from exploitation, transportation, and usage of coal, oil, and natural gas are defined as IFF_{CH4}. For methane sectors related to enteric fermentation and manure, landfills and waste and rice agriculture are defined as AGW_{CH4}.

Spatially resolved $\delta^{13}C$-CH_4 and uncertainty estimation. Spatially resolved distributions of $\delta^{13}C$-CH_4 source signatures for major methane categories were applied in this study: coal, natural gas/oil, livestock, wetlands, and biomass burning. For the other sources, including agricultural waste, rice, geological sources, termites, freshwater systems, and wild animals, we use a globally averaged value (Table S4) from a global inventory database that collected isotopic source signatures based on literature values [36,66,68].

Emission scenarios. An emission scenario is a combination of the individual CH_4 source estimates listed in Table S1. The annual total net CH_4 sources can be expressed as follows:

$$S_{tot} = S_{IFF} + S_{AGW} + S_{WET} + S_{BB} + S_{GEO} + S_{OTH} - S_{soil} \quad (6)$$

where S represents the individual CH_4 source from Table S1 and S_{soil} is a constant soil sink. The total number of emission scenarios is 96, calculated as 4 IFF_{CH4} x 3 AWG_{CH4} x 2 WET_{CH4} x 2 BB_{CH4} x 2 GEO_{CH4}. For each emission scenario, we use Monte Carlo techniques to estimate the uncertainty in the source signature propagated from bottom-up estimates and the spatial variability of the source signature. A set of 1000 random maps of $\delta^{13}C$-CH_4 values for each major CH_4 source (Table 1) were generated based on the uncertainty maps in this study assuming a Gaussian distribution. For CH_4 sources that are not spatially resolved, 1000 samples of the global-representative signature values are calculated with mean and 1-standard deviation defined by observations from the compiled databases (Table S4). One thousand sets of emission-weighted hemispheric time series of $\delta^{13}C$-CH_4, which were calculated with bottom-up estimates depending on emission scenarios, were used as inputs for the box model. For each emission scenario, the simulated time series of $\delta^{13}C$-CH_4 values covers the uncertainty range of spatial variability in the isotopic signatures of major CH_4 categories.

Data availability: All data needed to evaluate the conclusions in the paper are present in the paper and/or the Supplementary Materials. Additional ancillary data are available from the corresponding author upon request.

Code availability: The box model code in R (v.3.3.2) and data are publicly available at https://github.com/yuisheng/BoxModel_R_20200520. The custom R (v.3.3.2) code written to analyze and plot the data are fully available from the corresponding author upon request.

Acknowledgments: We thank AJ Turner for sharing the basis of our box model, G Janssens-Maenhout et al. for sharing the EDGAR inventories, and O Sherwood for sharing the database of □^{13}C-CH_4 signatures. We thank S.

Schwietzke, N. Chandra, and S. Strode for their constructive comments. JGC and AS thank the support of the Australian National Environmental Science Program-Earth Systems and Climate Change Hub. We thank University of Colorado's Institute of Arctic and Alpine Research INSTAAR (https://instaar.colorado.edu) and NOAA Earth System Research Laboratory (ESRL) (https://www.esrl.noaa.gov) for sharing the atmospheric $\delta^{13}C$-CH_4 measurements.

Funding: We acknowledge support from the Strategic Priority Research Program of the Chinese Academy of Sciences (XDA19040504 and XDA19070204) and the Gordon and Betty Moore Foundation through Grant GBMF5439 'Advancing Understanding of the Global Methane Cycle' supporting the Methane Budget released by the Global Carbon Project (globalcarbonproject.org). PKP is partly supported by the Environment Research and Technology Development Fund (JPMEERF20182002) of the Environmental Restoration and Conservation Agency of Japan.

Supplementary Data

Supplementary Data is available at NSR online.

Conflict of interest statement

None

References

1. Ocko IB, Sun T, Shindell D *et al.* Acting rapidly to deploy readily available methane mitigation measures by sector can immediately slow global warming. *Environ Res Lett* 2021;**16**:054042.

2. Meinshausen M, Vogel E, Nauels A *et al.* Historical greenhouse gas concentrations for climate modelling (CMIP6). *Geoscientific Model Development* 2017;**10**:2057–116.

3. Nisbet EG, Manning MR, Dlugokencky EJ *et al.* Very Strong Atmospheric Methane Growth in the 4 Years 2014–2017: Implications for the Paris Agreement. *Global Biogeochemical Cycles* 2019:2018GB006009.

4. Ferretti DF. Unexpected Changes to the Global Methane Budget over the Past 2000 Years. *Science* 2005;**309**:1714–7.

5. Saunois M, Stavert AR, Poulter B *et al.* The Global Methane Budget 2000–2017. *Earth System Science Data* 2020;**12**:1561–623.

6. Nisbet EG, Dlugokencky EJ, Bousquet P. Methane on the Rise--Again. *Science* 2014;**343**:493–5.

7. Thompson RL, Nisbet EG, Pisso I *et al.* Variability in Atmospheric Methane From Fossil Fuel and Microbial Sources Over the Last Three Decades. *Geophysical Research Letters* 2018;**45**:11,499-11,508.

8. Yin Y, Chevallier F, Ciais P *et al.* Accelerating methane growth rate from 2010 to 2017: leading contributions from the tropics and East Asia. *Atmospheric Chemistry and Physics* 2021;**21**:12631–47.

9. He J, Naik V, Horowitz LW *et al.* Investigation of the global methane budget over 1980–2017 using GFDL-AM4.1. *Atmospheric Chemistry and Physics* 2020;**20**:805–27.

10. Zhang Y, Jacob DJ, Lu X *et al.* Attribution of the accelerating increase in atmospheric methane during 2010–2018 by inverse analysis of GOSAT observations. *Atmospheric Chemistry and Physics* 2021;**21**:3643–66.

11. Schaefer H, Fletcher SEM, Veidt C *et al.* A 21st-century shift from fossil-fuel to biogenic methane emissions indicated by $^{13}CH_4$. *Science* 2016;**352**:80–4.

12. Schwietzke S, Sherwood OA, Bruhwiler LMP *et al.* Upward revision of global fossil fuel methane emissions based on isotope database. *Nature* 2016;**538**:88–91.

13. Worden JR, Bloom AA, Pandey S *et al.* Reduced biomass burning emissions reconcile conflicting estimates of the post-2006 atmospheric methane budget. *Nature Communications* 2017;**8**:2227.

14. Rigby M, Montzka SA, Prinn RG *et al.* Role of atmospheric oxidation in recent methane growth. *Proceedings of the National Academy of Sciences* 2017;**114**:5373–7.

15. Turner AJ, Frankenberg C, Wennberg PO *et al.* Ambiguity in the causes for decadal trends in atmospheric methane and hydroxyl. *Proceedings of the National Academy of Sciences* 2017;**114**:5367–72.

16. Saunois M, Bousquet P, Poulter B *et al.* Variability and quasi-decadal changes in the methane budget over the period 2000–2012. *Atmospheric Chemistry and Physics* 2017;**17**:11135–61.

17. Turner AJ, Frankenberg C, Kort EA. Interpreting contemporary trends in atmospheric methane. *Proceedings of the National Academy of Sciences* 2019;**116**:2805–13.

18. Nisbet EG, Fisher RE, Lowry D *et al.* Methane Mitigation: Methods to Reduce Emissions, on the Path to the Paris Agreement. *Reviews of Geophysics* 2020;**58**:e2019RG000675.

19. Nisbet EG, Dlugokencky EJ, Manning MR *et al.* Rising atmospheric methane: 2007-2014 growth and isotopic shift: rising methane 2007-2014. *Global Biogeochemical Cycles* 2016;**30**:1356–70.

20. Wolf J, Asrar GR, West TO. Revised methane emissions factors and spatially distributed annual carbon fluxes for global livestock. *Carbon Balance and Management* 2017;**12**:16.

21. Lunt MF, Palmer PI, Feng L *et al.* An increase in methane emissions from tropical Africa between 2010 and 2016 inferred from satellite data. *Atmospheric Chemistry and Physics* 2019;**19**:14721–40.

22. Zhang Z, Zimmermann NE, Calle L *et al.* Enhanced response of global wetland methane emissions to the 2015–2016 El Niño-Southern Oscillation event. *Environmental Research Letters* 2018;**13**:074009.

23. Janssens-Maenhout G, Crippa M, Guizzardi D *et al.* EDGAR v4.3.2 Global Atlas of the three major greenhouse gas emissions for the period 1970–2012. *Earth System Science Data* 2019;**11**:959–1002.

24. Höglund-Isaksson L. Bottom-up simulations of methane and ethane emissions from global oil and gas systems 1980 to 2012. *Environmental Research Letters* 2017;**12**:024007.

25. Helmig D, Rossabi S, Hueber J *et al.* Reversal of global atmospheric ethane and propane trends largely due to US oil and natural gas production. *Nature Geoscience* 2016;**9**:490–5.

26. Dalsøren SB, Myhre G, Hodnebrog Ø *et al.* Discrepancy between simulated and observed ethane and propane levels explained by underestimated fossil emissions. *Nature Geoscience* 2018;**11**:178–84.

27. Petrenko VV, Smith AM, Schaefer H *et al.* Minimal geological methane emissions during the Younger Dryas–Preboreal abrupt warming event. *Nature* 2017;**548**:443–6.

28. Hmiel B, Petrenko VV, Dyonisius MN *et al.* Preindustrial $^{14}CH_4$ indicates greater anthropogenic fossil CH_4 emissions. *Nature* 2020;**578**:409–12.

29. Etiope G, Ciotoli G, Schwietzke S *et al.* Gridded maps of geological methane emissions and their isotopic signature. *Earth Syst Sci Data* 2019;**11**:1–22.

30. Naik V, Voulgarakis A, Fiore AM *et al.* Preindustrial to present-day changes in tropospheric hydroxyl radical and methane lifetime from the Atmospheric Chemistry and Climate Model Intercomparison Project (ACCMIP). *Atmospheric Chemistry and Physics* 2013;**13**:5277–98.

31. Nicely JM, Canty TP, Manyin M *et al.* Changes in Global Tropospheric OH Expected as a Result of Climate Change Over the Last Several Decades. *Journal of Geophysical Research: Atmospheres* 2018;**123**:10,774-10,795.

32. Zhao Y, Saunois M, Bousquet P *et al.* Inter-model comparison of global hydroxyl radical (OH) distributions and their impact on atmospheric methane over the 2000–2016 period. *Atmospheric Chemistry and Physics* 2019;**19**:13701–23.

33. Naus S, Montzka SA, Patra PK *et al.* A three-dimensional-model inversion of methyl chloroform to constrain the atmospheric oxidative capacity. *Atmospheric Chemistry and Physics* 2021;**21**:4809–24.

34. Patra PK, Krol MC, Prinn RG *et al.* Methyl Chloroform Continues to Constrain the Hydroxyl (OH) Variability in the Troposphere. *Journal of Geophysical Research: Atmospheres* 2021;**126**:e2020JD033862.

35. Naus S, Montzka SA, Pandey S *et al.* Constraints and biases in a tropospheric two-box model of OH. *Atmospheric Chemistry and Physics* 2019;**19**:407–24.

36. Sherwood OA, Schwietzke S, Arling VA *et al.* Global Inventory of Gas Geochemistry Data from Fossil Fuel, Microbial and Burning Sources, version 2017. *Earth System Science Data* 2017;**9**:639–56.

37. Feinberg AI, Coulon A, Stenke A *et al.* Isotopic source signatures: Impact of regional variability on the $\delta^{13}CH_4$ trend and spatial distribution. *Atmospheric Environment* 2018;**174**:99–111.

38. Ganesan AL, Stell AC, Gedney N *et al.* Spatially Resolved Isotopic Source Signatures of Wetland Methane Emissions. *Geophysical Research Letters* 2018;**45**:3737–45.

39. Miller SM, Michalak AM, Detmers RG *et al.* China's coal mine methane regulations have not curbed growing emissions. *Nature Communications* 2019;**10**:303.

40. Poulter B, Bousquet P, Canadell JG *et al.* Global wetland contribution to 2000–2012 atmospheric methane growth rate dynamics. *Environmental Research Letters* 2017;**12**:094013.

41. Bloom AA, Bowman KW, Lee M *et al.* A global wetland methane emissions and uncertainty dataset for atmospheric chemical transport models (WetCHARTs version 1.0). *Geoscientific Model Development* 2017;**10**:2141–56.

42. Taylor KE. Summarizing multiple aspects of model performance in a single diagram. *Journal of Geophysical Research: Atmospheres* 2001;**106**:7183–92.

43. Umezawa T, Brenninkmeijer CAM, Röckmann T *et al.* Interlaboratory comparison of ^{13}C and d δD measurements of atmospheric CH_4 for combined use of data sets from different laboratories. *Atmospheric Measurement Techniques* 2018;**11**:1207–31.

44. Bruhwiler LM, Basu S, Bergamaschi P *et al.* U.S. CH_4 emissions from oil and gas production: Have recent large increases been detected?: U.S. Emissions From Oil and Gas Production. *Journal of Geophysical Research: Atmospheres* 2017;**122**:4070–83.

45. Hristov AN, Harper M, Meinen R *et al.* Discrepancies and Uncertainties in Bottom-up Gridded Inventories of Livestock Methane Emissions for the Contiguous United States. *Environmental Science & Technology* 2017;**51**:13668–77.

46. Bousquet P, Ciais P, Miller JB *et al.* Contribution of anthropogenic and natural sources to atmospheric methane variability. *Nature* 2006;**443**:439–43.

47. Andela N, Morton DC, Giglio L *et al.* A human-driven decline in global burned area. *Science* 2017;**356**:1356–62.

48. Chang J, Peng S, Ciais P *et al.* Revisiting enteric methane emissions from domestic ruminants and their $\delta^{13}CCH_4$ source signature. *Nature Communications* 2019;**10**:3420.

49. McCalley CK, Woodcroft BJ, Hodgkins SB *et al.* Methane dynamics regulated by microbial community response to permafrost thaw. *Nature* 2014;**514**:478–81.

50. Sweeney C, Dlugokencky E, Miller CE *et al.* No significant increase in long-term CH_4 emissions on North Slope of Alaska despite significant increase in air temperature: long-term CH_4 emissions on north slope. *Geophysical Research Letters* 2016;**43**:6604–11.

51. Oh Y, Zhuang Q, Liu L *et al.* Reduced net methane emissions due to microbial methane oxidation in a warmer Arctic. *Nature Climate Change* 2020;**10**:317–21.

52. Hopcroft PO, Valdes PJ, O'Connor FM *et al.* Understanding the glacial methane cycle. *Nature Communications* 2017;**8**:14383.

53. Zhang Z, Zimmermann NE, Stenke A *et al.* Emerging role of wetland methane emissions in driving 21st century climate change. *Proceedings of the National Academy of Sciences* 2017;**114**:9647–52.

54. Delwiche KB, Knox SH, Malhotra A *et al.* FLUXNET-CH_4 : a global, multi-ecosystem dataset and analysis of methane seasonality from freshwater wetlands. *Earth System Science Data* 2021;**13**:3607–89.

55. Koffi EN, Bergamaschi P, Alkama R *et al.* An observation-constrained assessment of the climate sensitivity and future trajectories of wetland methane emissions. *Science Advances* 2020;**6**:eaay4444.

56. Zazzeri G, Lowry D, Fisher RE *et al.* Carbon isotopic signature of coal-derived methane emissions to the atmosphere: from coalification to alteration. *Atmospheric Chemistry and Physics* 2016;**16**:13669–80.

57. Vinson DS, Blair NE, Ritter DJ *et al.* Carbon mass balance, isotopic tracers of biogenic methane, and the role of acetate in coal beds: Powder River Basin (USA). *Chemical Geology* 2019;**530**:119329.

58. Lunt MF, Palmer PI, Lorente A *et al.* Rain-fed pulses of methane from East Africa during 2018–2019 contributed to atmospheric growth rate. *Environmental Research Letters* 2021;**16**:024021.

59. Pandey S, Houweling S, Lorente A *et al.* Using satellite data to identify the methane emission controls of South Sudan's wetlands. *Biogeosciences* 2021;**18**:557–72.

60. Sapart CJ, Monteil G, Prokopiou M *et al.* Natural and anthropogenic variations in methane sources during the past two millennia. *Nature* 2012;**490**:85–8.

61. Tans PP. A note on isotopic ratios and the global atmospheric methane budget. *Global Biogeochemical Cycles* 1997;**11**:77–81.

62. Curry CL. Modeling the soil consumption of atmospheric methane at the global scale: soil consumption of atmospheric methane. *Global Biogeochemical Cycles* 2007;**21**:GB4012.

63. Murguia-Flores F, Arndt S, Ganesan AL *et al.* Soil Methanotrophy Model (MeMo v1.0): a process-based model to quantify global uptake of atmospheric methane by soil. *Geoscientific Model Development* 2018;**11**:2009–32.

64. Ni X, Groffman PM. Declines in methane uptake in forest soils. *Proceedings of the National Academy of Sciences* 2018;**115**:8587–90.

65. Strode SA, Wang JS, Manyin M *et al.* Strong sensitivity of the isotopic composition of methane to the plausible range of tropospheric chlorine. *Atmospheric Chemistry and Physics* 2020;**20**:8405–19.

66. Lassey KR, Etheridge DM, Lowe DC *et al.* Centennial evolution of the atmospheric methane budget: what do the carbon isotopes tell us? *Atmos Chem Phys* 2007:21.

67. Rice AL, Butenhoff CL, Teama DG *et al.* Atmospheric methane isotopic record favors fossil sources flat in 1980s and 1990s with recent increase. *Proceedings of the National Academy of Sciences* 2016;**113**:10791–6.

68. Lassey KR, Ragnauth S. Balancing the global methane budget: constraints imposed by isotopes and anthropogenic emission inventories. *Journal of Integrative Environmental Sciences* 2010;**7**:97–107.

69. Warwick NJ, Cain ML, Fisher R *et al.* Using δ^{13}C-CH_4 and δD-CH_4 to constrain Arctic methane emissions. *Atmos Chem Phys* 2016;**16**:14891–908.

70. Monteil G, Houweling S, Dlugockenky EJ *et al.* Interpreting methane variations in the past two decades using measurements of CH4 mixing ratio and isotopic composition. *Atmos Chem Phys* 2011;**11**:9141–53.

71. Prather MJ, Holmes CD, Hsu J. Reactive greenhouse gas scenarios: Systematic exploration of uncertainties and the role of atmospheric chemistry. *Geophysical Research Letters* 2012;**39**, DOI: 10.1029/2012GL051440.

72. Nicely JM, Salawitch RJ, Canty T *et al.* Quantifying the causes of differences in tropospheric OH within global models: Quantifying Global Model OH Differences. *Journal of Geophysical Research: Atmospheres* 2017;**122**:1983–2007.

73. Pandey S, Houweling S, Krol M *et al.* Influence of Atmospheric Transport on Estimates of Variability in the Global Methane Burden. *Geophysical Research Letters* 2019;**46**:2302–11.

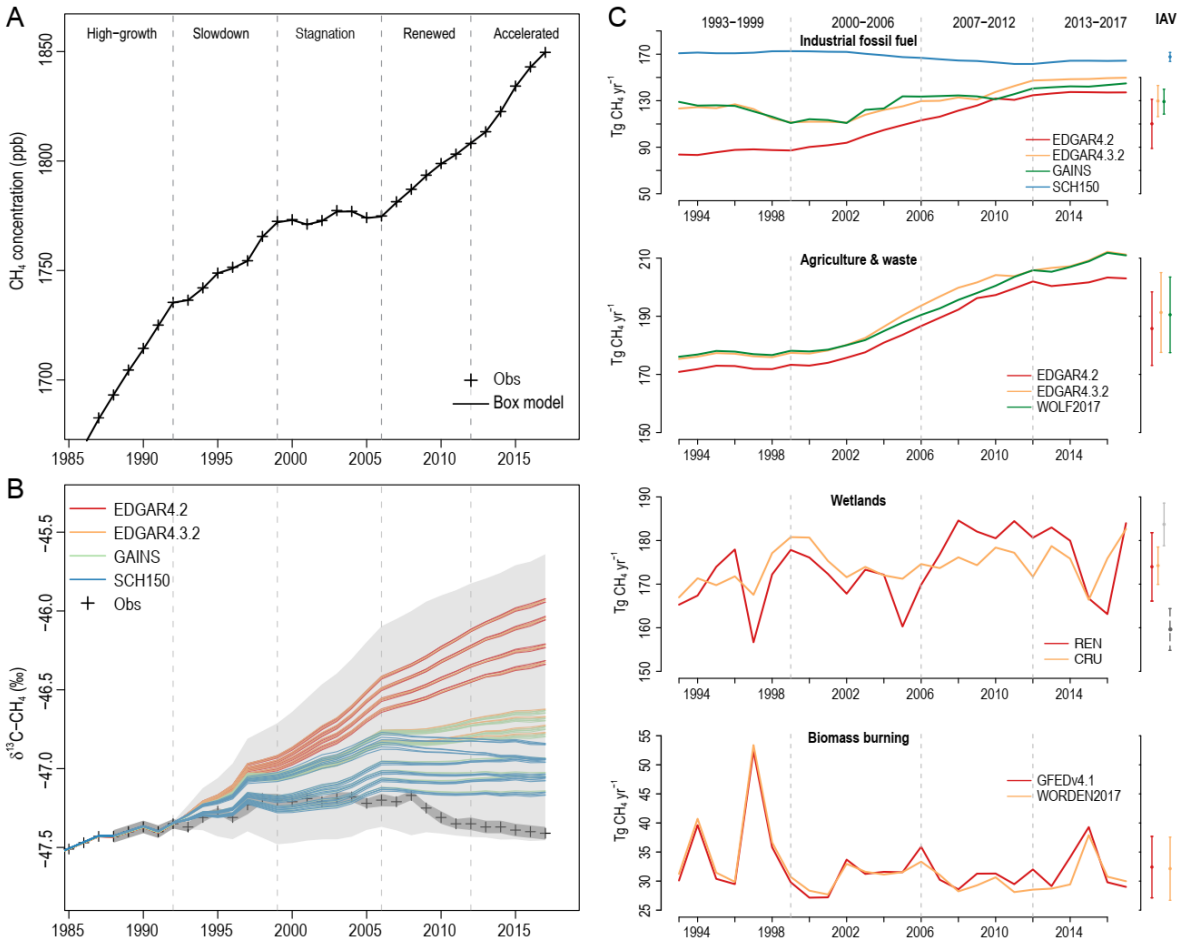

Figure 1. Simulated global atmospheric CH_4 concentration, $\delta^{13}C$-CH_4 values, and bottom-up estimates of major CH_4 sources. a, Simulated atmospheric CH_4 concentration (black solid line) from all emission scenarios exactly reproducing the observed CH_4 records (cross dots). The ensemble simulations of the box model were run in forward mode with prescribed $\delta^{13}C$-CH_4 variations from emission scenarios using OH time series derived from inverse mode (Fig. S1). **b**, Simulated ensemble mean $\delta^{13}C$-CH_4 values (colored solid lines) for emission scenarios grouped by industrial fossil fuel inventories (EDGARv4.2, EDGARv4.3.2, GAINS, and SCH150) in comparison to the observed global mean $\delta^{13}C$-CH_4 (cross). The uncertainty range of ensemble simulations (N = 96,000) and 1-σ uncertainty of the observations are shown as light gray areas and dark gray areas, respectively. **c**, Time series of annual total emissions for major sources. The interannual variability (1-σ) in CH_4 for each individual bottom-up estimate is shown at the right of the plot. Note that for the wetland category, the dashed bars represent two independent estimates from a bottom-up ensemble of wetland models [40] for 2000-2012 (light gray) and WetCHARTs [41] (dark gray) for 2001-2015.

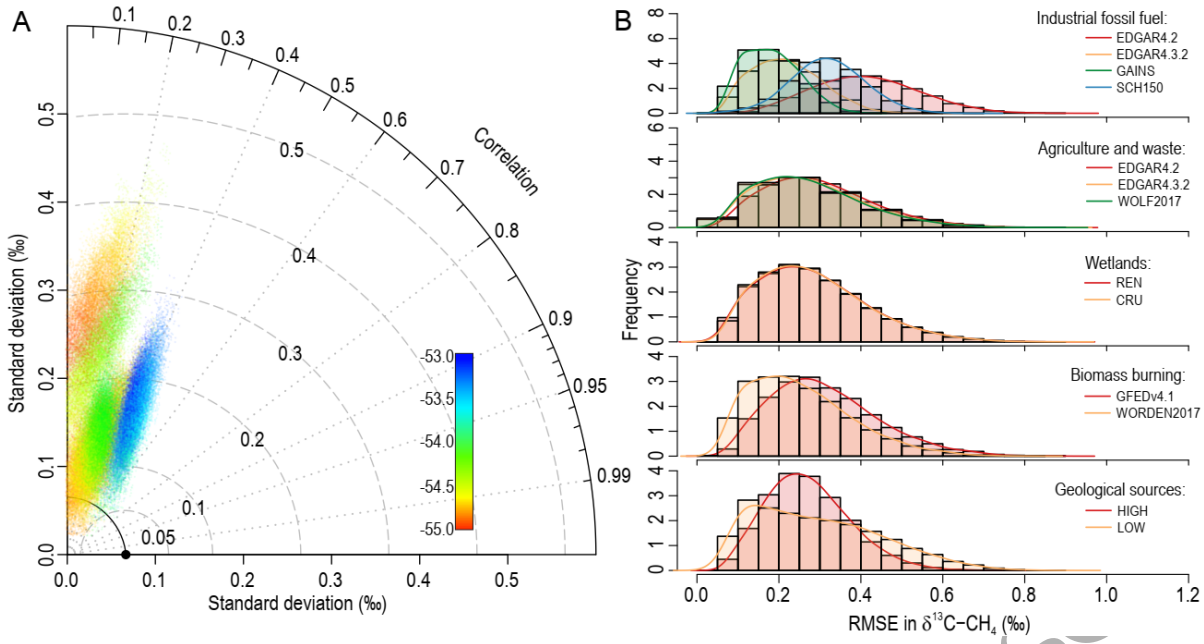

Figure 2. Performance of emission scenarios in simulating atmospheric δ^{13}C-CH_4. a, Taylor diagram illustrating the similarity between individual time series from the 96,000 simulations of different emission scenarios (colored dots) to the observed atmospheric δ^{13}C-CH_4 for 1993-2017. 'Obs' (black dot) refers to the observed global average δ^{13}C-CH_4 for 1993-2017. Each dot symbol indicates the correlation value (angle), the SD (radial distance to the origin point), and the RMSE (distance to the point marked 'Obs'), with different colors representing the mean global average δ^{13}C-CH_4 value of the source. **b,** Histograms of RMSE between simulated δ^{13}C-CH_4 values and observations grouped by bottom-up estimates with different colors for major CH_4 source categories. The solid lines represent the fitted density distribution after spline smoothing.

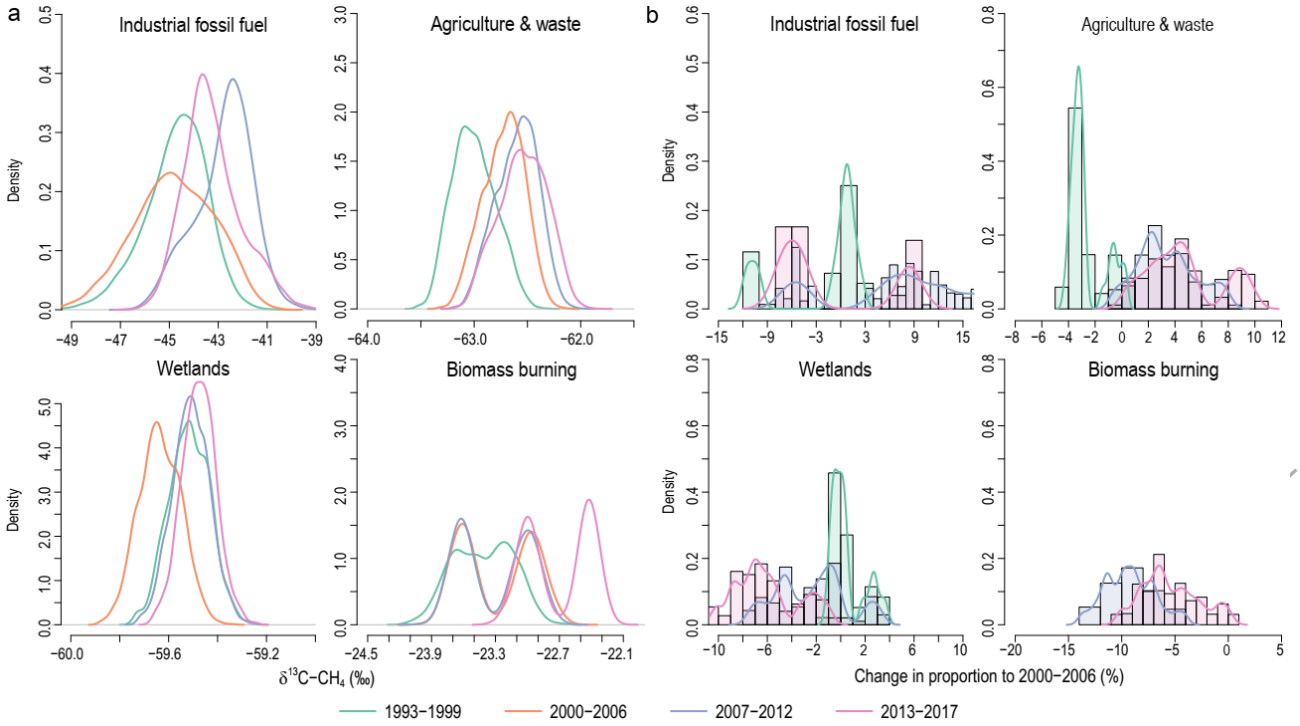

Figure 3. Changes in δ^{13}C-CH_4 values and in contribution of $^{13}CH_4$ mass to annual total for major source categories during 1993-2017. a. Density function of mean emission-weighted δ^{13}C-CH_4 value of the sources for four time periods from Monte Carlo accounting (N = 96,000): decreased atmospheric growth from 1993-1999, relative stabilization from 2000-2006, renewed growth from 2007-2012, and accelerated growth from 2013-2017. While the emission-weighted δ^{13}C-CH_4 signatures may change over time, it is the combination of these signatures with their respective emission amounts that determines the atmospheric isotopic trend. b. Density distribution of changes in the contribution of $^{13}CH_4$ mass from major CH_4 source categories to annual global $^{13}CH_4$ mass. The contribution of $^{13}CH_4$ mass is calculated as the average percentage change of the ratio of average annual total $^{13}CH_4$ mass in the source during 1993-1999, 2007-2012, and 2013-2017 relative to the CH_4 plateau period 2000-2006.

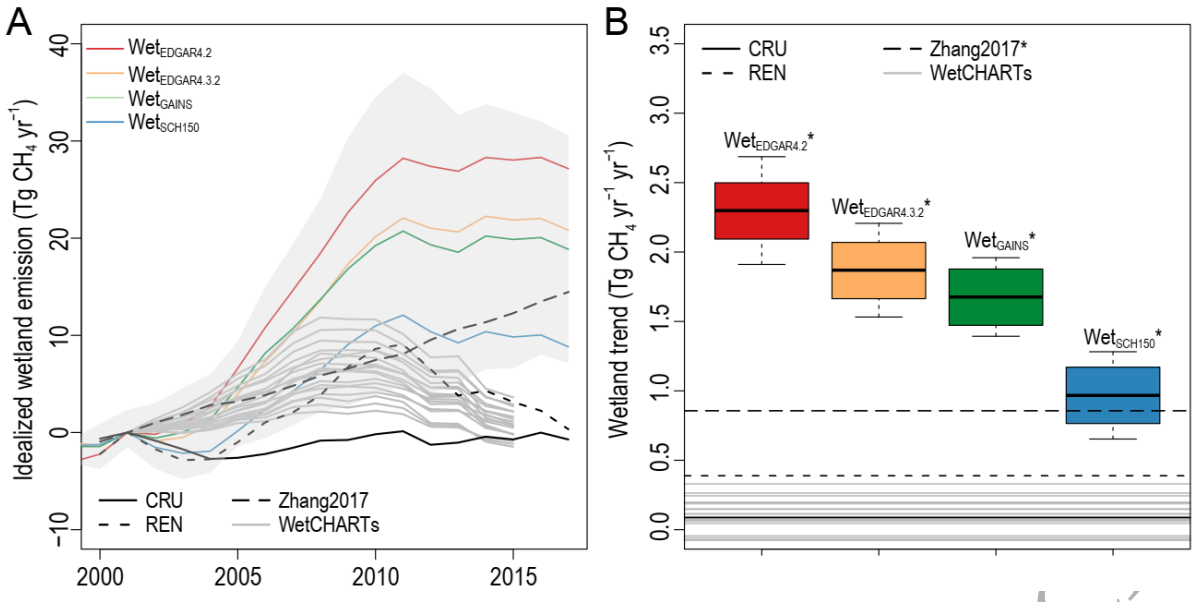

Figure 4. Idealized wetland emissions that reproduce the observations of atmospheric CH_4 and $\delta^{13}C$-CH_4 values for 2000-2017. (A) Time series of anomalies of idealized WET_{CH4} with a 7-year moving window (colored lines: ensemble mean grouped by IFF_{CH4}) in comparison to the two emission scenarios (CRU and REN) applied in this study and the estimates from [53] (denoted Zhang2017) and WetCHARTs [41]. All estimates are anomalies relative to 2001. The min/max range of idealized wetland emissions is shown as the gray area. (B) Trend of wetland emissions for 2000-2017 computed using linear regression. Significant trends at the 95% confidence level are denoted with "*".

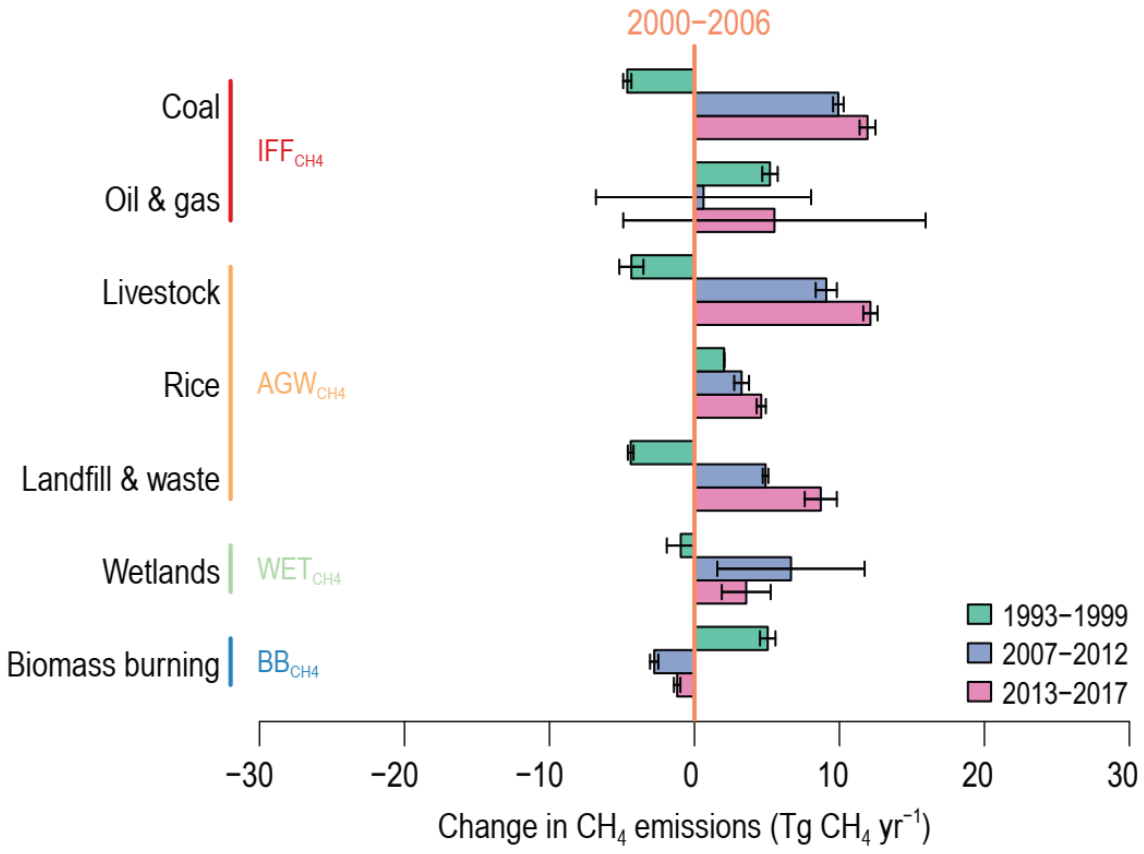

Figure 5. Changes in average total CH_4 emissions in the most likely scenarios. The changes in CH_4 emissions over the three periods are calculated relative to the average in the CH_4 plateau period 2000-2006 (vertical reference line in orange). The most likely scenarios are defined as the subset of emission scenarios (N = 960) in the 1st percentile lowest mean squared difference (MSD) (Fig. S6) in comparison to the full ensembles (N = 96,000; Fig. S9). IFF_{CH4}, AGW_{CH4}, WET_{CH4}, and BB_{CH4} represent the CH_4 sectors of industrial fossil fuels, agriculture and waste, wetlands, and biomass burning, respectively.

Table 1. Statistics of global representative average $\delta^{13}C\text{-}CH_4$ values for the major CH_4 categories used in the Monte Carlo simulations for 1993-2017. The interannual variability (IAV), uncertainty propagated from bottom-up estimates, and the full uncertainty that considers both uncertainty from emissions and spatially resolved distribution of source signatures for different CH_4 categories are listed. See Table S2 for CH_4 sectors that are not shown here.

$\delta^{13}C\text{-}CH_4$ (‰)	Mean	IAV	Uncertainty from emissions	Full Uncertainty
Coal	-45.8	0.71	1.23	2.57
Oil & gas	-43.8	0.06	0.61	0.93
Livestock	-65.4	0.16	0.32	0.86
Wetlands	-59.6	0.10	0.15	0.20
Biomass Burning*	-23.9	0.38	0.03	0.14

*The higher IAV of BB_{CH4} than the uncertainty range is due to the spikes during some extreme El Niño years, which are one order of magnitude higher than that in most of the years.